

# Three-dimensional interaction of waves and porous coastal structures using OpenFOAM®. Part II: Application

Pablo Higuera, Javier L. Lara, Inigo J. Losada\*

Environmental Hydraulics Institute "IH Cantabria", Universidad de Cantabria, C/Isabel Torres n° 15, Parque Científico y Tecnológico de Cantabria, 39011 Santander, Spain

## ARTICLE INFO

### Article history:

Received 16 April 2013

Received in revised form 10 September 2013

Accepted 16 September 2013

Available online 5 October 2013

### Keywords:

CFD

RANS

OpenFOAM

Wave–structure interaction

Two phase flow

Porous media

## ABSTRACT

This paper and its companion Higuera et al. (2014–this issue) introduce the formulation of Volume-Averaged Reynolds-Averaged Navier–Stokes (VARANS) equations in OpenFOAM® to simulate two-phase flow through porous media. This new implementation, so-called IHFOAM, corrects the limitations of the original OpenFOAM® code. An innovative hybrid methodology (2D–3D) is presented to optimize the simulation time needed to assess the three-dimensional effects of wave interaction with coastal structures. The combined use of a 2D and a 3D model enables the practical application of the 3D VARANS code to simulate real cases, contributing to a significant speed-up. This is highly convenient and especially suitable for non-conventional structures, as it overcomes the limitations inherent to applying semi-empirical formulations out of their range or 2D simulations only. A detailed study of stability and overtopping for a 3D porous high-mound breakwater at prototype scale subjected to oblique irregular (random) waves is carried out. Pressure around the caissons, overtopping discharge rate and turbulent magnitudes are presented in three dimensions. The mean pressure laws present a high degree of accordance with the formulation provided by Goda–Takahashi. Furthermore, local effects due to three-dimensional processes play a significant role, especially close to the breakwater head.

© 2013 Elsevier B.V. All rights reserved.

## 1. Introduction

The study of wave-induced three-dimensional processes interacting with coastal structures has been traditionally addressed testing scale models physically in a laboratory, and less frequently, instrumenting real structures. Such procedure usually involves an experimental facility, a large amount of time and work for the construction process and the adequate sampling instruments, yielding a high cost.

The numerical models can be used to assist the laboratory work (e.g. to dimension the structure prior to building the scale model). They can also be applied to extend the range of physical simulations after the tests have ended. Furthermore, the numerical simulations can be applied at prototype scale, thus avoiding the scale effects. However, as it was shown in the first part of this work (Higuera et al., 2014–this issue), the numerical simulations have to be calibrated according to experimental tests to obtain optimal results.

Until less than a decade ago only two-dimensional models were used for these purposes, because the computing power was barely enough to run them and to obtain results in a reasonable time. These models included 2DV Navier–Stokes (NS) equations (e.g. Guaniche et al., 2009; Lara et al., 2008; Losada et al., 2008b), 2DH Boussinesq equations (e.g. Losada et al., 2008a; Wei and Kirby, 1995) and 2DH Nonlinear Shallow Water equations (e.g. Hu et al., 2000; Zijlema and Stelling, 2011) among others. The 2DV models can solve the vertical

variations of pressure and velocity, hence they can accurately simulate nonlinear interaction between waves and wave breaking processes. They are limited to normal wave incidence, though. The 2DH models are depth-integrated, therefore they cannot solve vertical profiles, because their main assumption is hydrostatic pressure distribution. They can treat waves in shallow water regime really well, but not dispersive ones as accurately. For the same reasons, wave breaking has to be triggered artificially. However, they can offer oblique incidence.

The main drawback of these pioneering approaches is that they are two-dimensional, while the processes derived from the interaction between waves and coastal structures are essentially three-dimensional (e.g. wave generation, wave transformation over a real bathymetry, wave reflection and diffraction around a structure, overtopping and finally wave breaking).

Nowadays there is an increasing demand for three-dimensional simulations. This is not only a direct effect of the computational resources becoming cheaper and most powerful than ever, but also because numerical simulations have gained popularity as they have proven to be very valuable instruments. In this fashion, placing any number of probes and in any disposition is probably one of the most versatile features they can offer, as it can be carried out with very little effort and without disturbing the flow.

Another factor to take into account is the advances in wave generation and absorption, which improve the accuracy of the results directly from the base. Currently the most real three dimensional, directional irregular waves can be generated. The most classic approach involves using source functions and sponge layers or dissipative zones (Ha et al.,

\* Corresponding author.

E-mail address: [losadai@unican.es](mailto:losadai@unican.es) (I.J. Losada).

2013; Jacobsen et al., 2012). However, the size of the domain is increased by some fraction of the wavelength, which adds significant computational cost to the case. The other approach is to use Dirichlet-type boundary conditions to generate and absorb the waves, as in the works presented by Luppés et al. (2010), del Jesus et al. (2012) and Higuera et al. (2013a), which does not noticeably alter the computational cost.

Furthermore, 3D RANS codes have already been used to analyse a small number of processes and typologies providing accurate solutions (Higuera et al., 2013b; Lara et al., 2012). However, its use is not generalized yet and its validation is not as broad as the one available for 2DV models.

This paper is the continuation of another (Higuera et al., 2014–this issue), in which a new model called IHFOAM, which solves the VARANS equations and includes turbulence modelling, is developed from OpenFOAM® and validated for two-phase porous media flow interacting with porous structures.

The present work is structured as follows. After this introduction, a 2D–3D hybrid methodology to calculate the variables linked to the ultimate limit state of a structure is presented. This approach rationalizes the way to obtain these effects by simulating only the most relevant wave group within a sea state. The case of study, a long crested irregular sea state interaction with a high mound breakwater, is described next. Then, the numerical setup, first for the 2D model and second for the 3D model is presented. After that, the results of the 2D model are studied and used to feed IHFOAM. Finally, stability, overtopping and turbulence variables from the 3D simulation at prototype scale are analysed. To conclude, the conclusions of this work are highlighted.

## 2. Three-dimensional simulation of a vertical breakwater

Once the numerical model has been tested against laboratory data and proven to accurately represent the processes involved (Higuera et al., 2014–this issue), a three-dimensional structure at prototype scale is now simulated.

### 2.1. Methodology

Three-dimensional RANS models require a relatively large computational power to run. However, as we have shown so far in the first part of this work (Higuera et al., 2014–this issue) and in Higuera et al. (2013b), the run times can be reasonable.

Nevertheless, if we were designing a non-conventional coastal structure based on the standards, we would have to run at least an irregular sea state of 1 h, which at a typical simulation rate of 2 s per hour will take 75 days, a very long time for practical purposes. Furthermore, the output data can be relatively large in each time step.

A solution is proposed here, by applying a 2D–3D hybrid methodology which not only will shorten the time and resources needed, but will also overcome the current limitations inherent to applying semi-empirical formulations or 2D simulations only.

The first step is to run a 2DV RANS simulation using the IH2VOF model (Lara et al., 2011; Losada et al., 2008a), which has proven to yield accurate results. A 1 hour irregular (random) sea state generated for the design wave height, period and frequency dispersion is selected and tested. The structure is numerically monitored throughout the whole simulation, so the variables linked to the design limit state can be obtained, namely instantaneous safety factors for sliding and overturning.

A typical 2D simulation of 1 hour sea state at prototype scale with IH2VOF takes less than a day. The postprocessing time is negligible, as results can be obtained almost immediately after finishing the simulation. With the time series of pressures around the structure, the critical instant in terms of sliding and overturning can be obtained. From the experience, both of them occur almost at the same time, or within the same wave group. Very often, this is the group which includes the highest wave of the sea state, although this is not always true, due to wave propagation and non-linear interaction of waves. Locating precisely this wave group is the main purpose to run the 2D simulation.

The next step is to run the same simulation with IHFOAM, but restricted to the critical wave group. As the system starts from rest, the simulation should begin around 5 mean wave periods prior to the target waves, so that the system is already “warmed up” when they reach the structure.

Finally, once the 3D simulation is finished, the postprocessing procedure is carried out as usual, so the three-dimensional effects acting on the structure can be investigated.

### 2.2. Description of the case of study

The main objective of these purely numerical simulations is to test the influence of the wave incidence angle ( $30^\circ$ ) on the limit state design variables (i.e. instantaneous safety factors for sliding and overturning) of a high mound breakwater.

The structure is a high mound breakwater located at 20 m water depth. It has been designed using Goda–Takahashi formulation (Goda, 1985) as applied in Kim (2009, chap. 18) for a maximum wave height of 8.1 m and a significant wave period of 10 s.

A sketch of the breakwater is presented in Fig. 1. The caisson, which complies with the safety prescriptions against sliding and overturning, has 7 m below and 6 m above still water level. The primary armour layer consists of two layers of concrete cubes of side 1.7 m (mean weight of 13 tons). The berm is three pieces wide and lies submerged 2 m below the sea surface. The secondary layer is formed by two layers of rocks, with 0.8 m of nominal diameter (1.3 tons). The core is made of crushed rocks with a nominal diameter around 0.3 m. The estimated porosities are: 0.45 for the core, 0.5 for the secondary armour layer and 0.55 for the primary armour layer.

To simulate wave directionality the structure is rotated within the domain. This way the base mesh would be the same and waves would

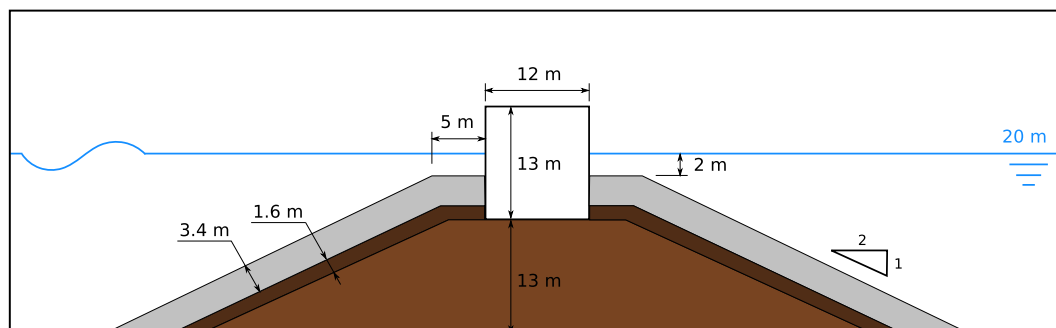


Fig. 1. Section of the high mound breakwater.

always be generated in identical manner regardless of the incidence angle.

### 2.3. 2D numerical setup

The numerical setup for IH2VOF corresponds to a slice of the hypothetical three-dimensional domain for  $0^\circ$  incidence angle, taking a plane normal to the Y axis. For the axes definition see Fig. 2. Since IH2VOF has its own meshing tool, the 2D and 3D meshes are generated independently. However, it is advised to mesh (or at least to sketch) the case in 3D first, so that both are as similar as possible in order to avoid a grid influence in the numerical simulations.

As sketched in Fig. 2, the caisson is placed 200 m away from the wave generation boundary (right wall). The outflow boundary with active wave absorption condition (Higuera et al., 2013a) is located 133 m leeside of the structure (left wall).

The mesh is composed of three zones in the X direction and two zones in the Z direction, with variable cell sizes. First, a wave propagation zone was prepared in the X direction, in which  $\Delta x$  varies from 1 m at the generation boundary to 0.25 m, 10 m away from the caisson. Next, a uniform zone in which  $\Delta x$  is equal to 0.25 m spans for 80 m. The width of this second zone is chosen so that the structure lies within it on the 3D mesh, for the  $30^\circ$  rotation angle. Finally, a 75 m long zone leads to the absorbing boundary, grading the cell size from 0.25 m to 1 m. In the Z axis the vertical cell size varies from 0.5 m near the bottom to 0.25 m at the initial free surface level, and then it is maintained throughout the remaining height. The final mesh is orthogonal and conformal, and has less than 100,000 cells.

The wave forcing corresponds to an irregular sea state which follows a JONSWAP spectrum of  $H_s = 4.5$  m,  $T_p = 10$  s and  $\gamma = 3.3$ . The random waves have been obtained based on an iterative process, which ensures that the sea state obtained is representative of the parameters provided. This is done by obtaining a free surface series, carrying out an upcrossing analysis and comparing the obtained values for  $H_s$  and  $T_p$  with the theoretical ones. On top of that, an additional condition regarding the highest wave height on the sea state, which must be at least 1.8 times  $H_s$ , was checked. A 2% error is allowed.

The free surface elevation of the simulated sea state is presented in Fig. 3. An upcrossing analysis of the signal yields the maximum wave height: 8.04 m, which takes place at  $t = 1707$  s. Afterwards we will show that the greatest event in terms of the total dynamic force on the caisson is associated to this particular wave.

The closure terms in the VARANS equations are implemented differently in IH2VOF, therefore, there is no direct equivalence between the porous media parameters used in it and those applied in IHFOAM.

Hence, a set of parameters which are known to work with rubble mound breakwaters was used. The estimated porosities and mean rock size previously introduced have been used.

The 1 hour sea state simulation is completed in less than 19 h.

### 2.4. 3D numerical setup

The numerical mesh is created around an impervious obstacle (i.e. the caisson). The first step is to create a base mesh. Then, the obstacle is removed using *snappyHexMesh* and finally snapped to the original surface for a better definition of the obstacle, yielding the final mesh.

The base mesh has the shape of a box ( $345 \times 225 \times 35$  m), and is orthogonal and conformal. It presents 3 zones in X, 2 zones in Y and 2 zones in Z, with variable cell size. Similarly to the 2D version, the zones in X and Z match. The major difference is that the discretization is half, so the cell sizes presented for the 2D case are multiplied by 2. Regarding the 2 zones in the Y direction, the first one spans for 135 m with constant resolution of 0.5 m, thus covering the area where the structure is located. Then, on the second zone, the  $\Delta y$  grows up linearly to 1 m, 90 m away from the end of zone 1. Once the base mesh is ready, the structure is removed without performing additional refinement around its surface, yielding a mesh with 10 million elements.

The smallest cell in the 3D mesh is a cube of side 0.5 m, hence, the resolution is not very good. If the size of all the cells was half they would be equal to the ones in the 2D case. However, the base mesh would have near 80 million elements, which would be very difficult to handle and would need enormous computational resources. A more convenient method is applied to obtain the required discretization: dynamic mesh refinement along the free surface.

The dynamic mesh refinement along the free surface is already provided in OpenFOAM®. Nevertheless, an improved version had to be developed so that it could be applied to meshes created with *snappyHexMesh*. The tool is integrated in the solver, and refines by splitting in halves the cells which the interface (defined as the cells where  $\alpha_1$  ranges from 0.01 to 0.99) between both phases is crossing and their immediate neighbours. An example can be seen in Fig. 4. It also handles un-refinement when necessary. This process takes place each 10 time steps and it is not fast, as it almost doubles the time it takes to calculate a regular time step. During the simulation the number of cells varies constantly, but a mean of 20 million is obtained for this case.

The waves are generated using the boundary conditions described in Higuera et al. (2013a). Wave generation linked with active wave absorption takes place at the boundary, using the spectral components which lead to the free surface elevation signal in Fig. 3. The phases have been shifted accordingly to start at  $t = 1625$  s in the IH2VOF

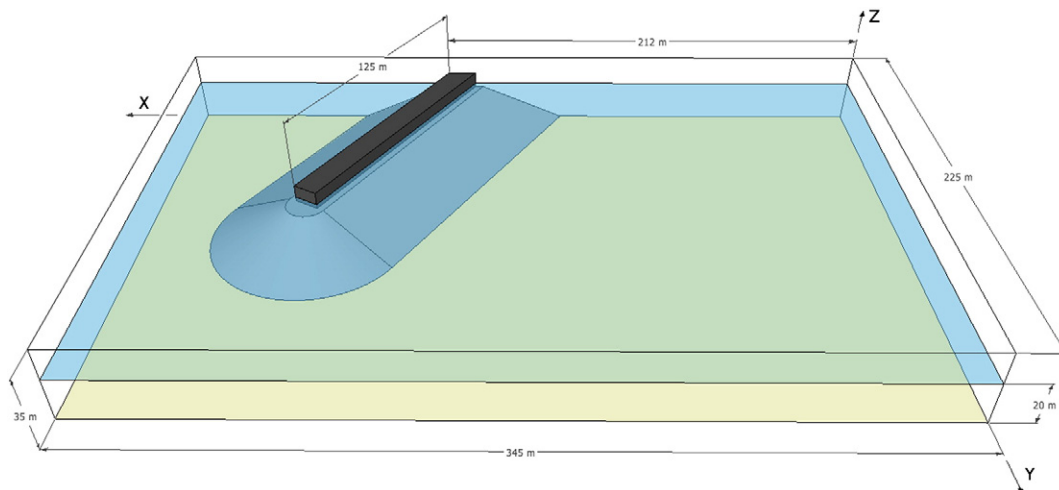


Fig. 2. Three-dimensional sketch of the domain and the breakwater.

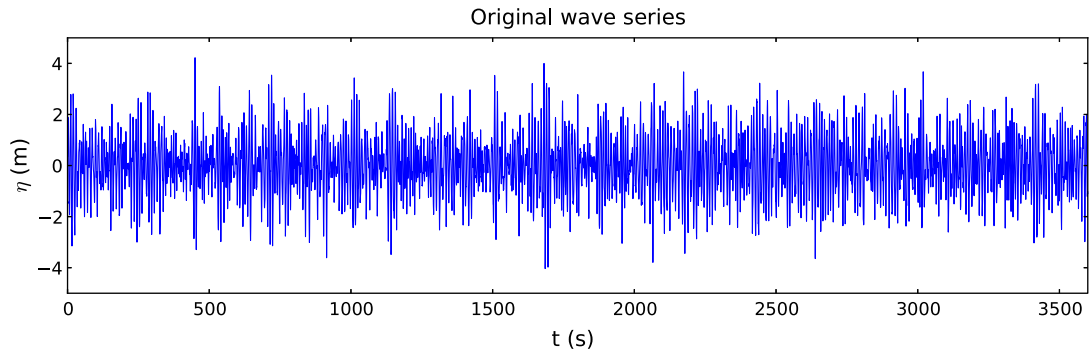


Fig. 3. Irregular sea state.

simulation time, other than that, the data that feed the model are identical. Ten individual slices of the boundary are considered to actively absorb the incoming waves independently while generating, so that free surface variations along the generation boundary due to the reflection pattern can be handled. The boundary opposite to wave generation is purely absorbent. It is also divided in 10 slices which work independently for the same reason. The lateral boundaries are set to a slip boundary condition, this way the incoming waves do not get distorted.

The turbulence is modelled using the porous  $k-\omega$  SST model (Higuera et al., 2014–this issue), which is applicable in cases in which large flow separation can be expected. In this case such process will most likely take place on the rubble mound and on the breakwater front. All the fields are stored each 1 s for the first 70 s of simulation. As this is the warming up time, no more resolution is needed. From  $t = 70$  s until the end of the simulation ( $t = 110$  s), all the fields are saved at 20 Hz.

The simulation rate is more or less 200 s per week, parallelizing the case into 96 processors (2.6 GHz).

### 2.5. 2D numerical results

As it has been mentioned before, the 2D simulation is run to calculate the critical instant for the structure in terms of sliding and overturning. The pressure time series around the structure are integrated to calculate the forces and moments to which the structure is subjected. Then the safety factors are calculated as follows:

$$C_{SD} = \mu \frac{W_{\text{Caisson}} - \text{Uplift}}{\sum F_{\text{Horizontal}}} \quad (1)$$

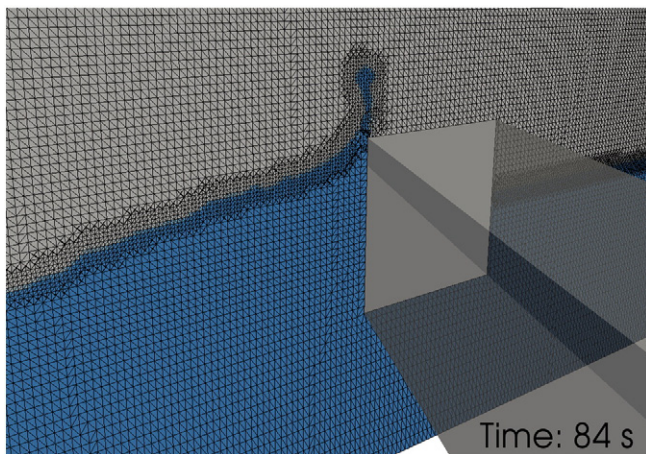


Fig. 4. Dynamic mesh refinement. Most of the cells are hexahedral, as the triangulation shown is only a visualizing artefact. Water is the dark phase, and air is the light phase.

$$C_{OT} = \frac{\text{Mom}_{\text{W. Caisson}}}{\sum \text{Mom}_{\text{Horizontal F.}} + \text{Mom}_{\text{Uplift}}} \quad (2)$$

where  $C_{SD}$  is the safety coefficient against sliding, in the same manner that  $C_{OT}$  is the one against overturning.  $W_{\text{Caisson}}$  is the weight of the caisson, Uplift denotes the uplift force and  $F_{\text{Horizontal}}$  considers the rest of the horizontal forces. Mom. stands for momentum, and the subscript indicates the force by which it is produced. Finally,  $\mu$  is the friction factor between the caisson and the core, which takes the typical value of 0.7.

The two-dimensional results are presented in Fig. 5. The sliding coefficient is shown in the upper panel, while the overturning coefficient is shown in the lower panel. The lower dashed line indicates the minimum threshold which may never be surpassed. The global minimum is marked with a circle. It can be noted that it occurs at the same time ( $t = 1707$  s) step for both panels, therefore we can conclude that in this particular case the limit state is linked to the highest wave group. This analysis yields the shifting time before the 3D simulation is started ( $t = 1625$  s, as already mentioned).

### 2.6. 3D numerical results

In this section the three-dimensional results for wave group interaction with a high mound breakwater are analysed. The breakwater is divided in 5 independent caissons of 25 m in length, as presented in Fig. 6.

The evolution of the safety coefficients against sliding and overturning is calculated for each of the caissons first. The dynamic pressure distribution is obtained all along the breakwater, considering 1 m long slices (i.e. 25 profiles per caisson) and a 10-cm resolution between points. The integration of the 3D pressure yields the forces and the moments that act on the caisson. Finally, the safety coefficients are calculated.

The safety coefficients (top panels) and dynamic forces (lower panels) for the five caissons are plotted in Fig. 7. As it can be seen, both safety coefficients (sliding represented as a continuous line and overturning as a dash-dot line, top panels) evolve similarly, having more or less the same shape when the seaside force presents a crest (see lower panels, in continuous line). The sliding coefficient decreases as well when a minimum in the seaside force is obtained, associated with a wave trough. However, the magnitude is smaller than for the previous case. It is remarkable that the uplift force (dotted line, lower panels) is in phase with the seaside force, while the leeside force (dash-dot line, lower panels) presents a phase lag dependent on the location of the caisson.

The minimum safety coefficients have been extracted and gathered in Table 1, along with the time of occurrence. For the first 4 caissons, the critical instant is associated to the first of the two high waves of the group. For the caisson number 5, which is located at the breakwater head, the second wave impact is of larger magnitude. Although the first impact is also considered, the second is the most critical and is named *Caisson 5 Prime*. The values in Table 1 show that the breakwater is

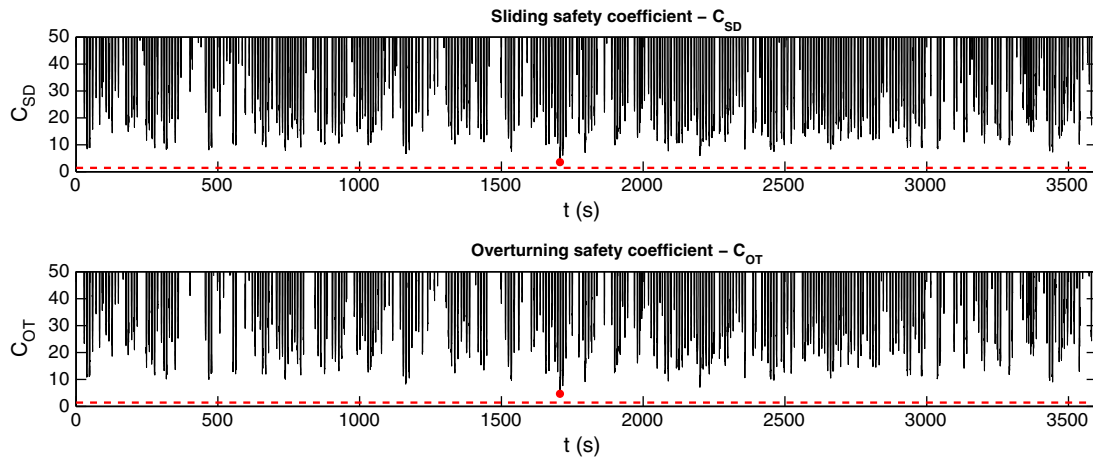


Fig. 5. Evolution of safety coefficients on the caissons for the 2D case. The global minimum is marked with a circle.

never in danger of failing for this design sea state, as the safety coefficients are larger by far than the 1.4 design value.

The Goda–Takahashi pressure distribution (Takahashi et al., 1994) has been calculated using the sea state significant wave height as a starting point and the 30° incidence correction angle (Tanimoto et al., 1976). There is also another factor that has been taken into account. The correction term presented in Burcharth and Liu (1999) [Eq. (5)] reduces the effective pressure acting on the caisson, as it takes into consideration that due to the oblique incidence the maximum pressure does not take place along the whole caisson at once. The calculation for long-crested waves yields a factor of 0.983, which is less than a 2% reduction.

Although the mean measured pressure distribution is close to the theoretical one, the formulation yields safety factors 3.3 and 3.34 for sliding and overturning, respectively. The theoretical sliding coefficient is systematically higher than the ones obtained numerically. This indicates that the three dimensional effects are not negligible, as they are not on the safe side.

Fig. 8 includes the seaward, leeward and uplift pressure distribution on each of the caissons for the most critical instant. The Goda–Takahashi expected pressure distribution for this incidence angle (dashed line) is also plotted. The mean numerical pressure is represented scaled as a dash-dot line, while the maximum and minimum pressures along the caisson are represented as dotted lines.

The seaside pressure laws for caissons 1 and 2 resemble in shape and magnitude of the theoretical approach by Goda and Takahashi. For the rest of the caissons the numerical pressure is noticeably smaller than the theoretical one, probably because of the three-dimensional effects induced by the reflection of the waves. Nevertheless, the first wave impact yields a consistent shape all along the breakwater. In general, the seaside pressure towards the top part of the face is smaller in the numerical model. This indicates that Goda–Takahashi predicts a higher run-up and splash. The uplift pressure is also systematically found smaller (from 20% to 50%) depending on the location. The second impact is shown for case *Caisson 5 Prime* (bottom right panel) only. The shape of the mean pressure is not so linear, but more pointed with smooth transitions, and large variations appear between the smallest and largest values. In fact the maximum pressure shows a very pronounced peak which almost doubles the pressure predicted by Goda–Takahashi.

In order to understand better the process of the waves impacting the caissons we may refer to Fig. 14, which will later be used to explain the overtopping pattern. This figure features snapshots of the first wave of the group, which causes the worst safety scenario for caissons 1–4, impacting on the structure. It is noticeable that this wave is not broken and it does not break onto the structure either. What is interesting to note is that the splash is turning backwards conforming the reflected wave which propagates away already broken (see  $t = 86$  and  $88$  s).

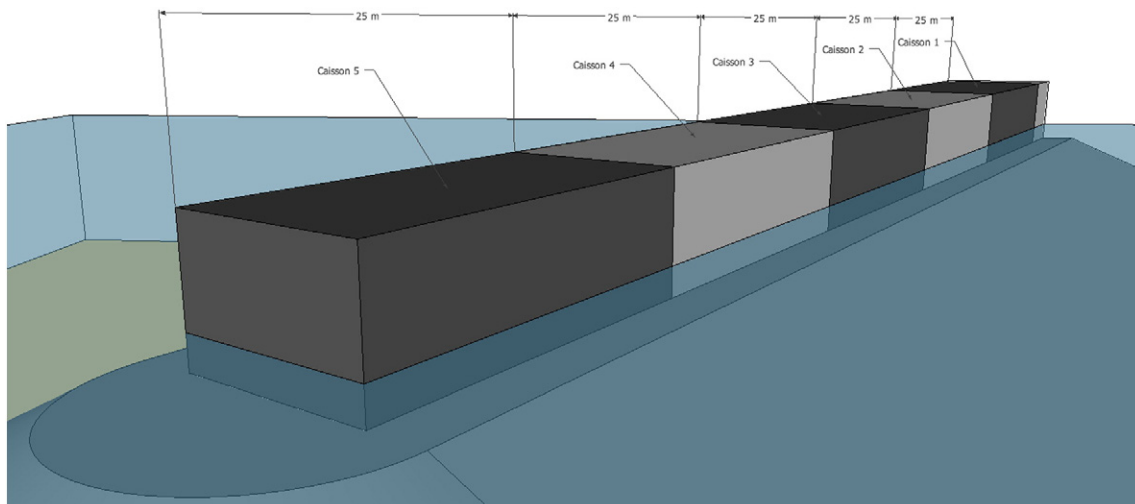


Fig. 6. Individual location of the caissons.

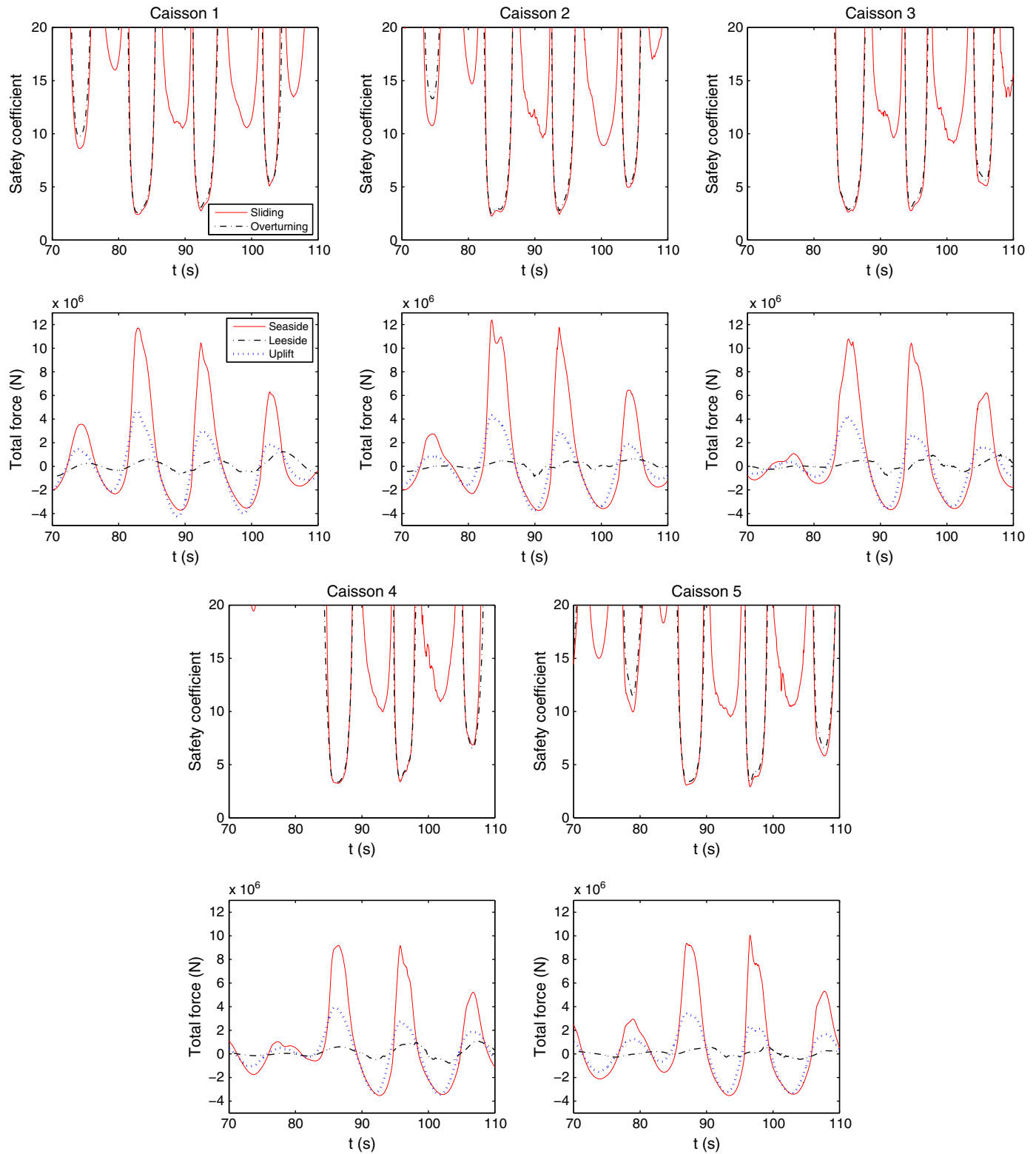


Fig. 7. Evolution of safety coefficients and total forces on the caissons.

The interaction between the reflected wave and the second wave of the group makes that the latter one arrives completely broken to the structure (barely visible in the centre of Fig. 13).

The time series of the dynamic pressure acting on the midpoint ( $X = 112.5$  m,  $Z_{local} = 6.5$  m) of the seaside wall of caisson 5 is presented in Fig. 9. The result is in accordance with the observations made in the previous paragraph regarding the two main waves. The first wave produces a

non-impulsive impact. The second wave presents a large spike, which is almost double than the subsequent sustained pressure, and is the result of a broken wave impact. This proves that even though IHFOAM is a solver for two incompressible phases, impulsive pressure peaks can be detected. Furthermore, treating the wave breaking in 3D makes the air to escape sideways (unlike in 2D simulations) when impacting, which yields a more realistic pressure distribution.

**Table 1**  
Minimum safety coefficients on the caissons.

	Sliding		Overturning	
	SC	t (s)	SC	t (s)
C1	2.39	82.3	2.59	82.3
C2	2.26	83.0	2.48	83.0
C3	2.64	84.6	2.86	84.65
C4	3.23	85.9	3.36	85.85
C5	3.08	86.45	3.36	86.45
C5'	2.92	95.95	3.35	95.95

In Fig. 10 the dynamic force acting on a vertical slice located in the middle of the seaside face of each caisson is presented in the left panel. The theoretical force given by the Goda–Takahashi formulation is represented in a horizontal red dashed line. The instantaneous dynamic pressure distribution on such slices for the instant with the largest force (marked with the vertical black dashed line in the left panel) is shown in the right panel. The first impact is more or less even throughout the whole structure, presenting small variations only, inherent to the three-dimensionality of the processes. The second wave is more interesting. It shows a peak resulting from the localized impulsive impact, and is decreasing towards the breakwater head, as the wave is losing height due to the local breaking process.

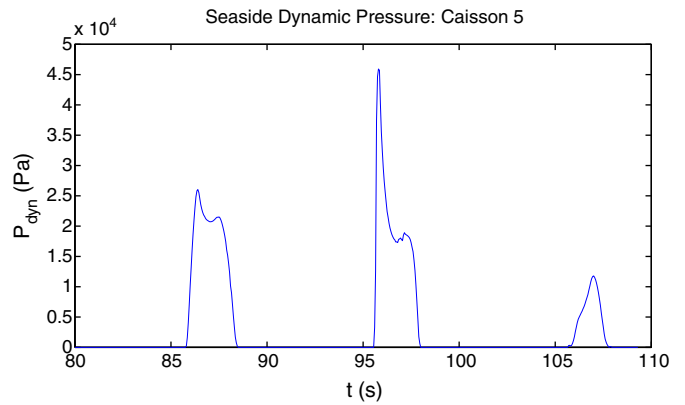


**Fig. 9.** Dynamic pressure in the midpoint ( $X = 112.5$  m,  $Z_{local} = 6.5$  m) of the seaside wall of caisson 5.

The instantaneous pressure distribution in the right panel (blue dots) is quite different from the ones shown in Fig. 8. The comparison with the Goda–Takahashi distribution, represented as a black dashed line, confirms the impulsive nature of the impact which can be inferred from the distinctive shape of the pressure law. However, as it has

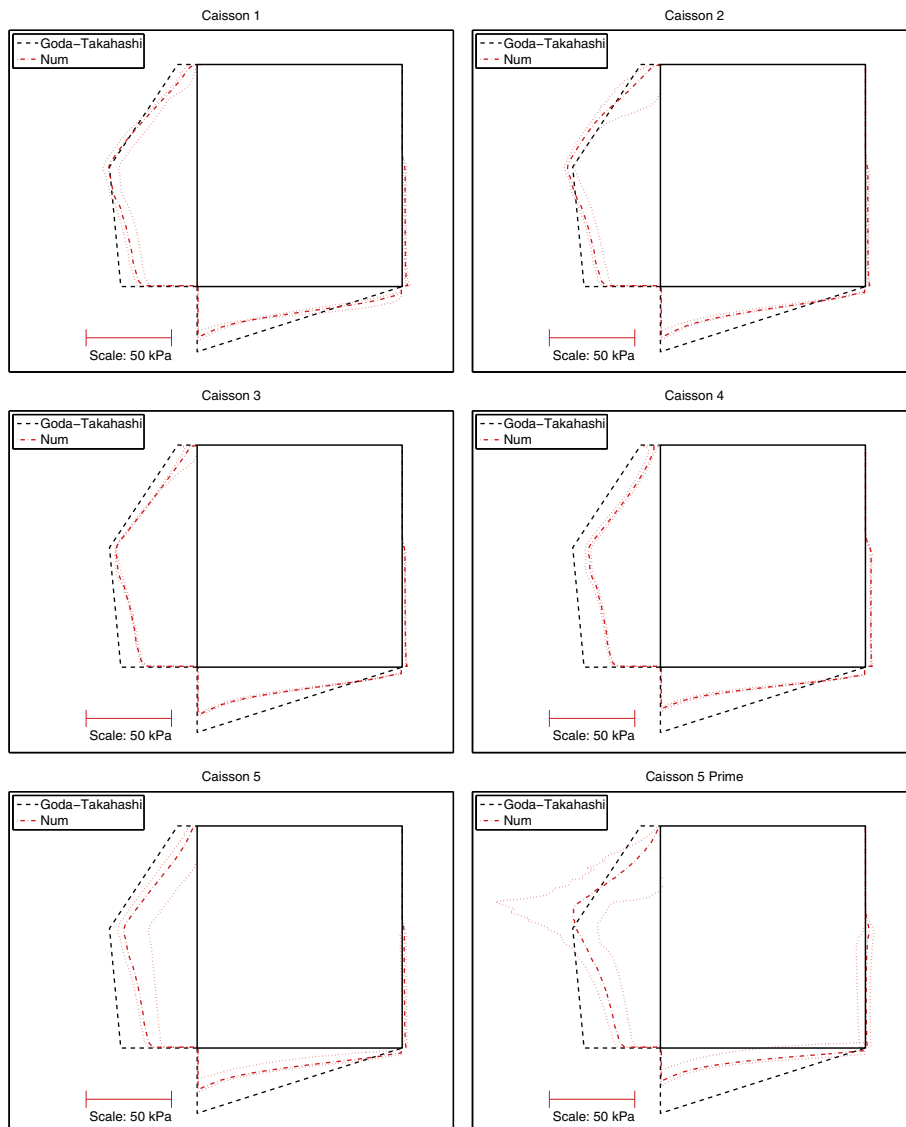


**Fig. 8.** Pressure distribution on the caissons for the most critical instant.

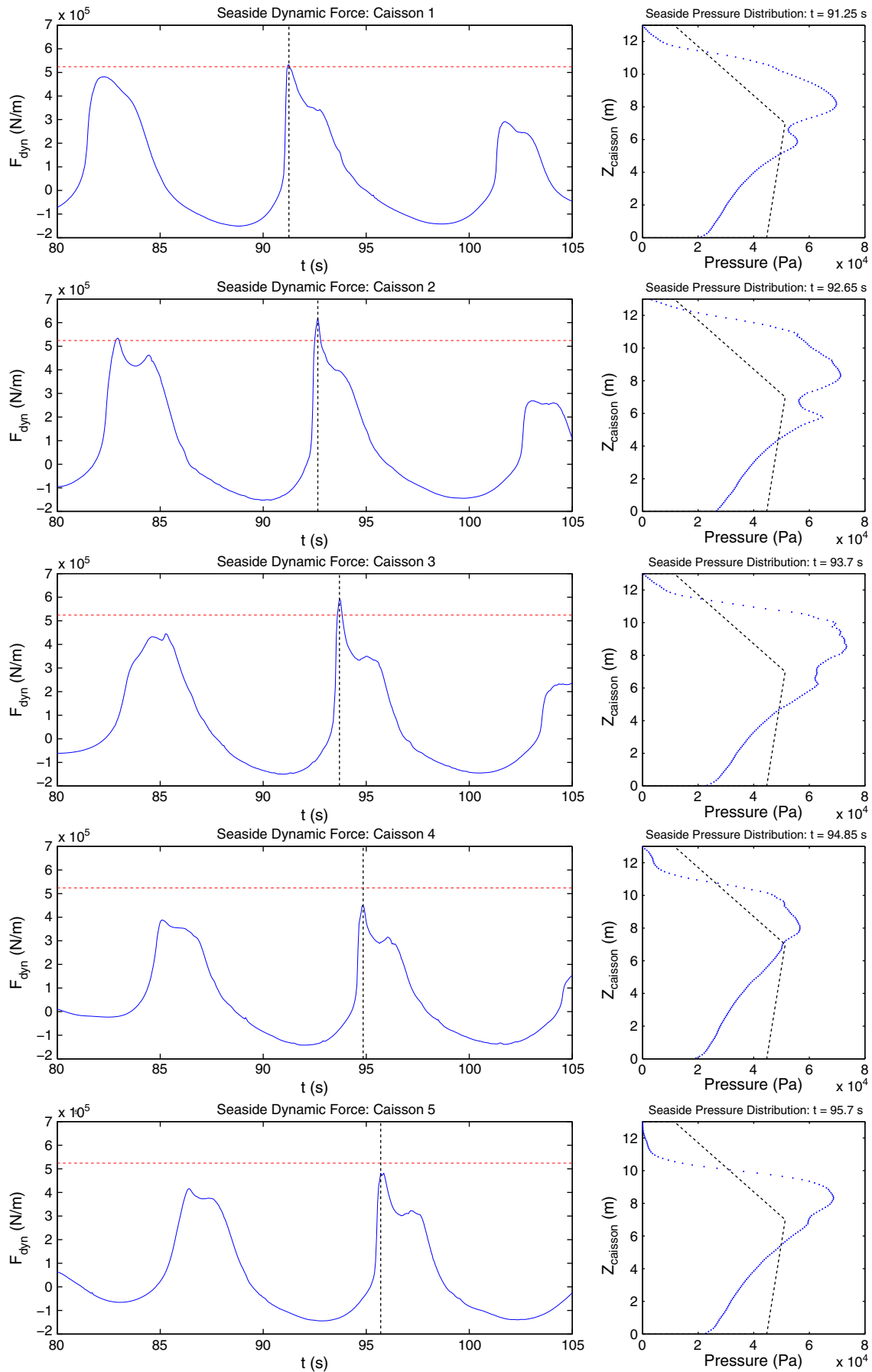


Fig. 10. Dynamic force acting on a vertical slice (left panel) and dynamic pressure distribution for the instant with the largest force (right panel).

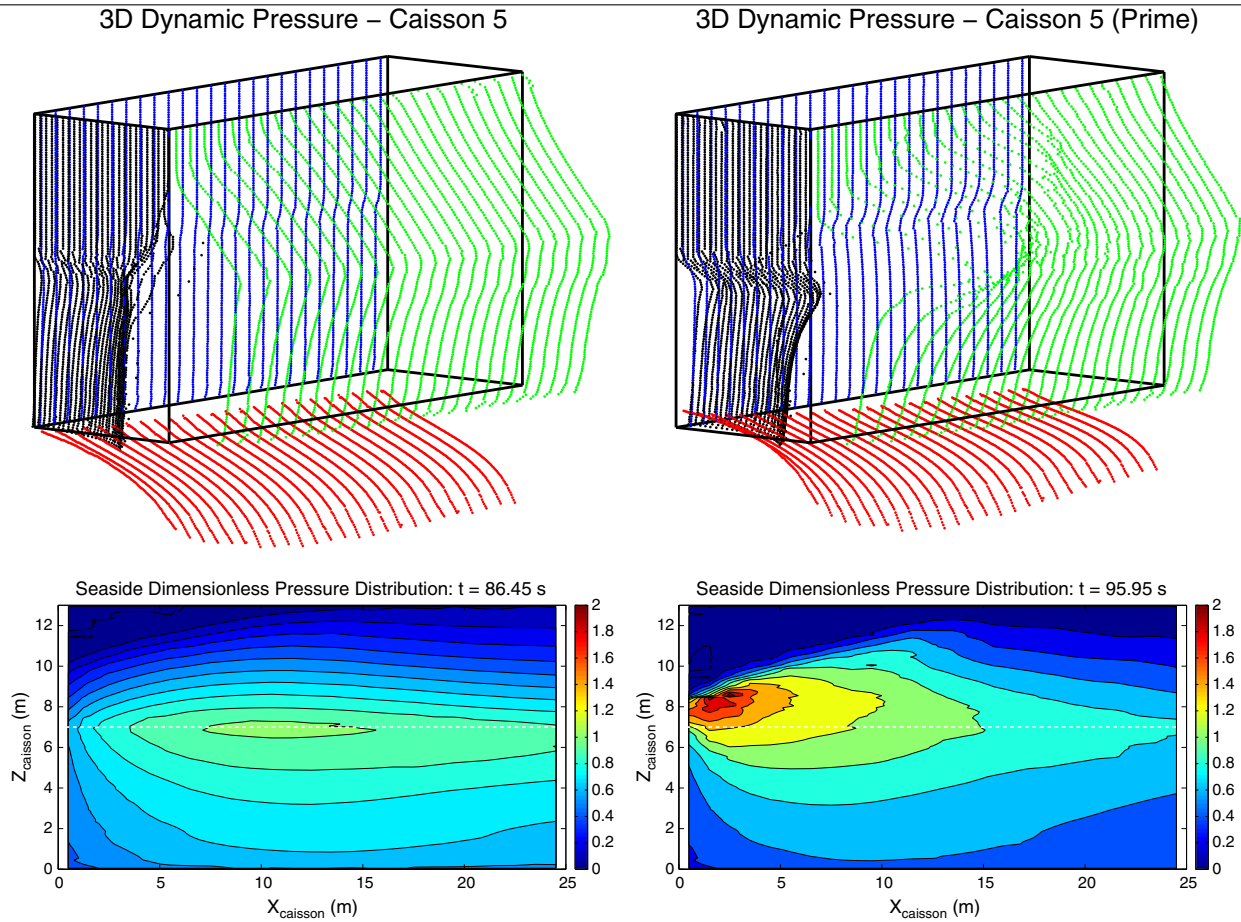


Fig. 11. 3D pressure distribution on caisson 5 for the two critical instants. Lower panel represented with a local coordinate system.

already been pointed out, the impulsive effects are so localized that the most restrictive safety factors occur for the first wave impact.

The difference between the impacts on caisson 5 (first wave) and 5 prime (second wave) is clearer in Fig. 11. In it the whole three-dimensional pressure distribution around the fifth caisson (top panel) and a contour of dimensionless dynamic pressure on the seaside wall ( $P_{dyn}/(\rho g H_s)$ , bottom panel) are plotted. The left panels show the first impact and the right panels show the second one. No pressure scale has been included because of the perspective, but the reader is either referred to the bottom panel or to Fig. 8 (lower panels) for an order of magnitude. The first impact presents an even pressure distribution throughout the seaside wall of the caisson, just showing a slight increase in pressure where the wave crest is located ( $X_{local}$  between 7.5 and 15 m), right at the initial water level (white dashed line). The second impact presents a large peak close to the end of the caisson, much larger in magnitude (almost double than on the left panel). The effect is very concentrated and located 1 m above the initial water level. The leeside and bottom faces do not show significant changes between both cases. However, the front wall presents a noticeable depression for the second impact due to the greater flow separation.

The evolution of the free surface around the structure for the first remarkable wave impact is shown in Fig. 12). The free surface is coloured according to the module of the water particle velocity. The wave starts to impact on the first caisson ( $t = 82$  s) and continues propagating towards the breakwater head. Overtopping can be observed starting at  $t = 84$  s encompassed with wave reflection, which propagates away from the caissons. Wave diffraction at the breakwater head can be distinguished in all the snapshots. The second high wave to reach the structure can be spotted in the last frame, interacting with the reflected wave prior to impacting the structure. The primary armour layer appears dry

on this last picture, towards the zone of caisson 1, due to the arrival of the wave trough.

A more detailed view of the strongest impact on caisson 5 is presented in Fig. 13. The incoming wave is already broken, and even some pockets of air are trapped and can be seen in the snapshot. This can also be inferred from the shape of the seaside force (Fig. 7, caisson 5, bottom panel). Therefore, the pressure distribution corresponds to impulsive loading.

The whole sequence of overtopping can also be observed in Fig. 13 starting from the breakwater head. First, the wave impacts and splash occurs. In this case it reaches 5 m above the crest level. The splash continues to advance and falls gradually, impacting the surface of the breakwater. Finally, it falls on the other side of the caisson.

A quantitative analysis of the overtopping is presented in Fig. 14. The instantaneous overtopping discharge rate is plotted as a function of the simulation time and the local coordinate on the breakwater. The caisson 1 starts at  $Dist = 0$  m and the caisson 5 ends at  $Dist = 125$  m. A total of 125 measurements have been taken over the breakwater at a 20 Hz sampling rate. The three-dimensional effects are clear. The first wave produces a maximum overtopping rate of around  $9 \text{ m}^3/\text{s}$  between the first two caissons. Then it is reduced drastically and becomes more or less even for the rest of the caissons ( $2.5 \text{ m}^3/\text{s}$ ). The second wave is influenced by the reflected wave, as the overtopping rate for the first caissons is cut almost a half. The rest of the caissons suffer from an increase of overtopping rate. The effect is more pronounced on the last caisson, in which it is almost triple. The results point out that overtopping is a magnitude highly dependent on the location and on the preceding waves, so in order to study it from a statistical point of view, very long simulations will be needed.

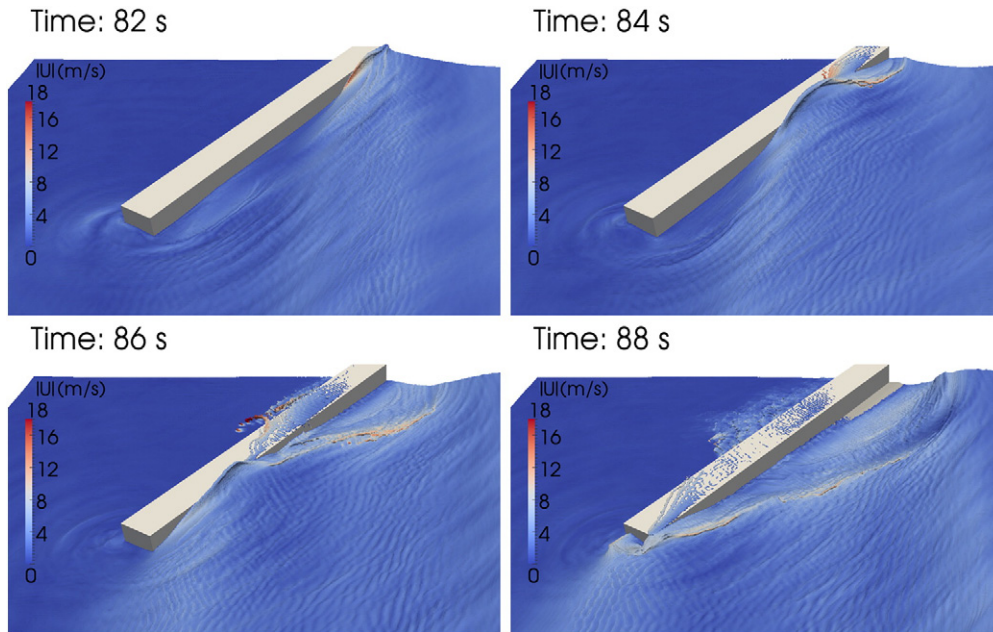


Fig. 12. Free surface around the breakwater for the critical wave impact and water particles velocity module.

Another relevant variable that can be studied is the velocity of water particles, as there are studies (Tørum, 1994) that correlate the velocity magnitude above the breakwater primary armour layer with the forces occurring at each of its elements.

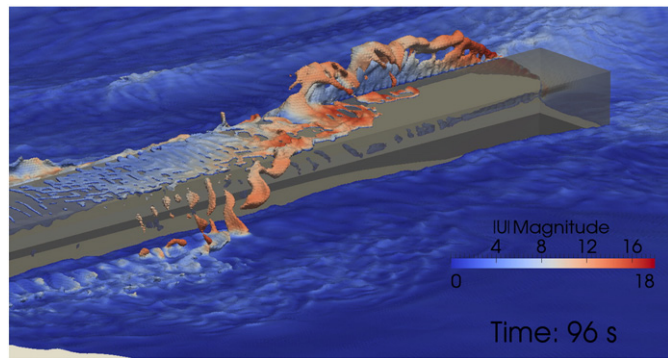


Fig. 13. Critical wave impact for caisson 5.

In the left panel of Fig. 15 the distribution of particle velocities on a plane 10 cm above the bottom is represented. The right panel shows the same situation but with a different colour scale, as the velocities on the outer layer of the breakwater are superposed. As expected, the velocity is lower inside the porous media and it continues to decrease until it reaches the core due to increasing frictional effects. The places where the horizontal particle velocity changes direction are easily distinguished with a dark blue colour, between the red zones. Trying to follow them from the top boundary of the figure yields to the conclusion that the water particle velocities increase above the porous media, due to the effective decrease in water depth.

The rocks are subjected to a velocity on the order of 2 m/s at this instant, which recalling from Fig. 13 corresponds to the critical state for caisson number 5. Two locations present high values: the breakwater head near the free surface, and the seaside berm, where the water is retreating. These results are promising and can lead to the analysis of stability of the armour layers.

Relevant turbulent variables around the structure are presented in Fig. 16. A number of slices of the domain have been obtained to better

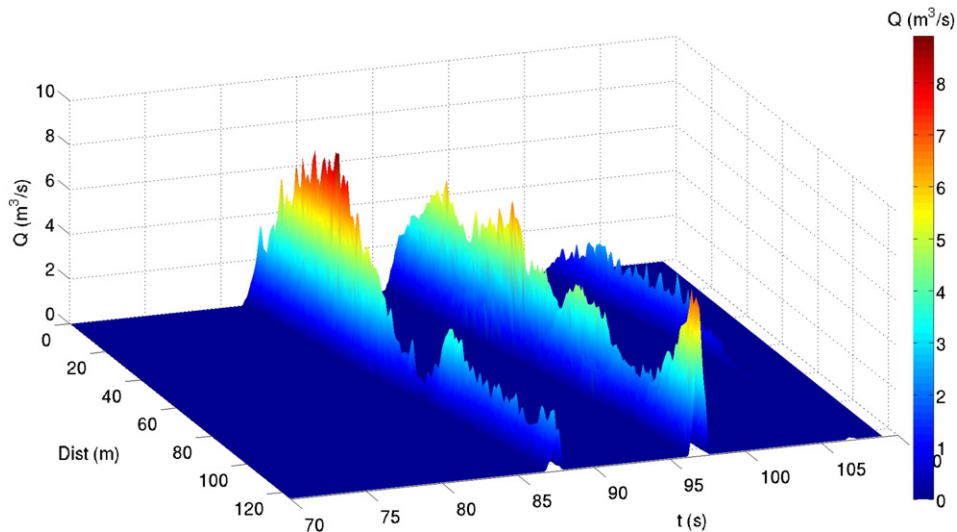


Fig. 14. Space-time series of instantaneous overtopping discharge rate.

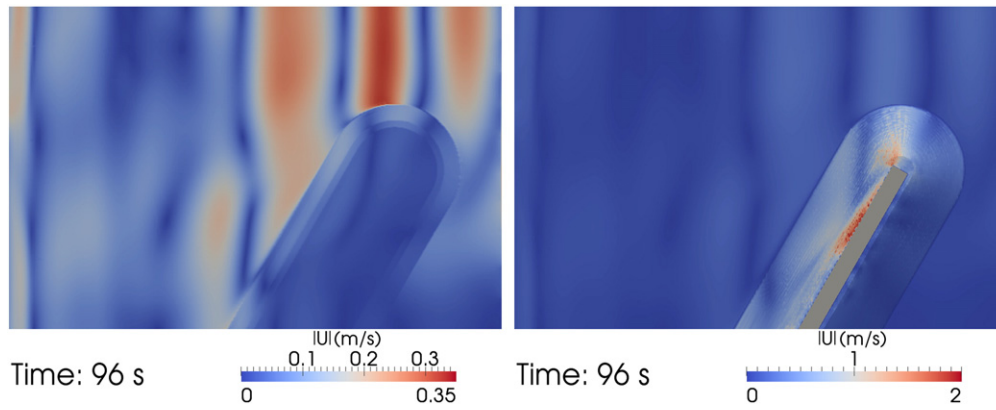


Fig. 15. Particle velocity distribution around the structure. Left panel: at 10 cm from the bottom. Right panel: at 10 cm from the bottom and on the primary armour layer.

visualize the results. The turbulent kinetic intensity ( $k$ ) is larger in the vicinity of the breakwater and close to the free surface, a result of the high turbulence levels in the air, induced by the overtopping events which have occurred and are occurring at that instant (see Fig. 12). No significant  $k$  levels are present inside the porous media, although on the first slice a part of the interface between the primary armour layer and the clear region shows a noticeable value. It can be concluded that the use of a  $k$ - $\omega$  SST model, which does not include the closure terms for the porous media, yields smaller dissipation inside the porous materials, unlike  $k$ - according to the results presented in the first part (Higuera et al., 2014–this issue).

Regarding  $\omega$  (turbulence eddy frequency), the values are not only high near the breakwater, but also throughout entire air region all over the domain. The region leeward the breakwater shows smaller  $\omega$  levels, as the agitation in that zone is not as high as in the exposed area. It is important to note that the  $\omega$  level increases due to the variation of porosity between the different layers of the breakwater.

### 3. Conclusions

In this paper and in its companion (Higuera et al., 2014–this issue) a new numerical model called IHFOAM, based on OpenFOAM®, has been developed to deal with real applications in coastal engineering. After validating the model, it has been applied to carry out the stability and overtopping analysis of a porous breakwater in three dimensions. The following conclusions can be extracted.

Recalling from the first part: IHFOAM has been developed to address the lack of rigorous treatment of two-phase porous media in OpenFOAM® (i.e. failure to conserve mass). The special boundary conditions for wave generation and active wave absorption presented in Higuera et al. (2013a) have also been included as part of the model. The VARANS equation implementation includes the  $k$ - and  $k$ - $\omega$  SST turbulence models.

An innovative hybrid methodology (2D–3D) has been presented in this second part to optimize the simulation time needed to check the three-dimensional effects of wave-induced pressure, overtopping and turbulence acting on coastal structures. A 1-hour sea state simulation carried out with the IH2VOF model allows to obtain the location of the group of waves which induces the most critical effects on the structure. This single group can be simulated next in IHFOAM, reproducing just a fraction of the initial sea state. This methodology results in a significant speed-up ( $\times 36$  approximately) in simulation time and in a rationalization of the computational resources.

The importance of this methodology is that it allows obtaining magnitudes linked to the limit state of coastal structures in 3D. The use of the 3D numerical simulations is specially indicated for cases where semi-empirical formulations and 2D simulations may not accurately represent the existent physical processes, as it overcomes most of the limitations of both. Furthermore, if it was not for the hybrid methodology proposed in here these sea-state-long simulations would be virtually unaffordable.

The high mound breakwater simulation yields highly three-dimensional results. The mean pressure laws present a high degree of accordance with the formulation provided by Goda–Takahashi. However, the safety coefficients obtained are, most of the times, lower than those from theory. This indicates that the three-dimensional effects are not negligible. Some impulsive forces are obtained for the second wave on the group, but they introduce limited local effects, so in general the lowest safety factors are induced by non-impulsive loads. The overtopping discharge rate is completely dependent on the location of the point, but also on the preceding waves. To obtain more significant results, long simulations must be carried out.

The turbulent kinetic intensity distribution is concentrated around the structure, where the largest values are present. This fact, along with the results of the previous part (Higuera et al., 2014–this issue) reveals that the turbulence is an important process to consider in coastal

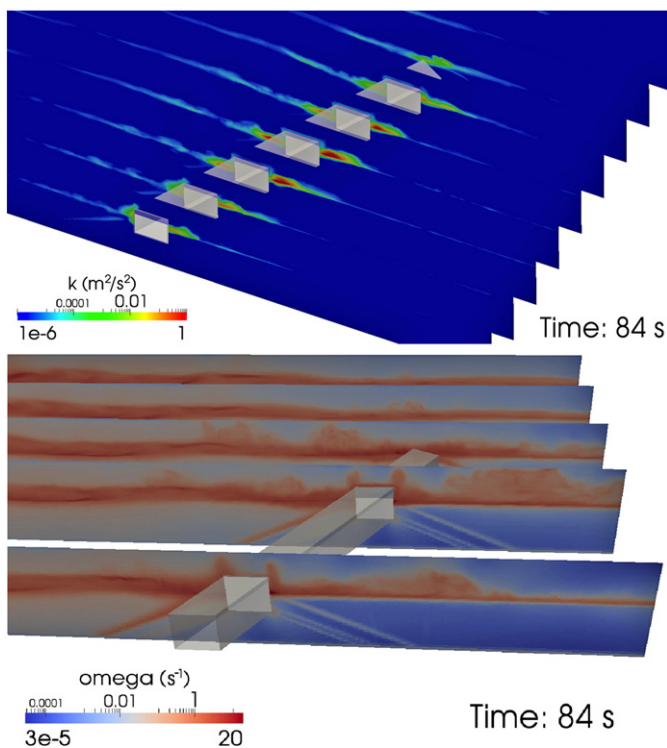


Fig. 16. Relevant turbulent variables around the structure. Waves come from the left.

engineering simulations, and especially when flow through porous media is present. The use of a  $k-\omega$  SST model, which does not include the closure terms for the porous media, yields smaller dissipation inside the porous materials, unlike  $k-\epsilon$ , for which closure terms are included.

Potential results for future studies regarding stability of the rubble mound have been shown. The model successfully shows, according to reality, that water velocities are smaller inside the porous media, and that the critical zones in terms of stability are the seaside berm and the front primary armour layer close to the free surface.

In short, IHFOAM has proved to be a valuable instrument to assess the three-dimensional effects in simulations which include complex sea states and porous media flow.

## Acknowledgements

Pablo Higuera is indebted to the Spanish Ministry of Education, Culture and Sports for the funding provided in the “Formación de Profesorado Universitario” Grant Program (FPU12-04354).

The work is funded by project BIA2011-26076 of the “Ministerio de Ciencia e Innovación” (Spain).

## References

- Burcharth, H.F., Liu, Z., 1999. Pulsating wave loads. Section 4.3: 3D Effects Force Reduction of Short-crested Non-breaking Waves on Caissons, vol. 2a. Technical University of Braunschweig.
- del Jesus, M., Lara, J.L., Losada, I.J., 2012. Three-dimensional interaction of waves and porous structures. Part I: numerical model formulation. *Coast. Eng.* 64, 57–72.
- Goda, Y., 1985. *Random Seas and Design of Maritime Structures*. University of Tokyo Press.
- Guanche, R., Losada, I.J., Lara, J.L., 2009. Numerical analysis of wave loads for coastal structure stability. *Coast. Eng.* 56, 543–558.
- Ha, T., Lin, P., Cho, Y.S., 2013. Generation of 3D regular and irregular waves using Navier–Stokes equations model with an internal wave maker. *Coast. Eng.* 76, 55–67.
- Higuera, P., Lara, J.L., Losada, I.J., 2013a. Realistic wave generation and active wave absorption for Navier–Stokes models: application to OpenFOAM. *Coast. Eng.* 71, 102–118.
- Higuera, P., Lara, J.L., Losada, I.J., 2013b. Simulating coastal engineering processes with OpenFOAM. *Coast. Eng.* 71, 119–134.
- Higuera, P., Lara, J.L., Losada, I.J., 2014. Three-dimensional interaction of waves and porous coastal structures using OpenFOAM. Part I: formulation and validation. *Coast. Eng.* 83, 243–258 (this issue).
- Hu, K., Mingham, C.G., Causon, D., 2000. Numerical simulation of wave overtopping of coastal structures using the non-linear shallow water equations. *Coast. Eng.* 41, 433–465.
- Jacobsen, N.G., Fuhrman, D.R., Fredsøe, J., 2012. A wave generation toolbox for the open-source CFD library: OpenFOAM. *Int. J. Numer. Methods Fluids* 70, 1073–1088.
- Kim, Y., 2009. *Handbook of Coastal and Ocean Engineering*. World Scientific.
- Lara, J.L., Losada, I.J., Guanche, R., 2008. Wave interaction with low mound breakwaters using a RANS model. *Ocean Eng.* 35, 1388–1400.
- Lara, J.L., Ruju, A., Losada, I.J., 2011. Reynolds averaged Navier–Stokes modelling of long waves induced by a transient wave group on a beach. *Proc. R. Soc. A* 467, 1215–1242.
- Lara, J.L., del Jesus, M., Losada, I.J., 2012. Three-dimensional interaction of waves and porous structures. Part II: model validation. *Coast. Eng.* 64, 26–46.
- Losada, I.J., Gonzalez-Ondina, J.M., Diaz, G., Gonzalez, E.M., 2008a. Numerical simulation of transient nonlinear response of semi-enclosed water bodies: model description and experimental validation. *Coast. Eng.* 55, 21–34.
- Losada, I.J., Lara, J.L., Guanche, R., Gonzalez-Ondina, J.M., 2008b. Numerical analysis of wave overtopping of rubble-mound breakwaters. *Coast. Eng.* 55, 47–62.
- Luppes, R., Veldman, A.E.P., Wellens, P.R., 2010. Absorbing boundary conditions for wave simulations around offshore structures. V European Conference on Computational Fluid Dynamics (ECOMAS CFD 2010), Lisbon.
- Takahashi, S., Tanimoto, K., Shimosako, K., 1994. A proposal of impulsive pressure coefficient for design of composite breakwaters. *Proceedings of the International Conference on Hydro-technical Engineering for Port and Harbour Construction*, pp. 489–504.
- Tanimoto, K., Moto, K., Ishizuka, S., Goda, Y., 1976. An investigation on design wave force formulae of composite-type breakwaters. *Proceedings of the 23rd Japanese Conference on Coastal Engineering*, pp. 11–16.
- Tørum, A., 1994. Wave induced forces on armor unit on berm breakwaters. *J. Waterw. Port Coast. Ocean Eng.* 120, 251–268.
- Wei, G., Kirby, J.T., 1995. Time-dependent numerical code for extended Boussinesq equations. *J. Waterw. Port Coast. Ocean Eng.* 121, 251–261.
- Zijlema, M., Stelling, G.S., 2011. Swash: an operational public domain code for simulating wave fields and rapidly varied flows in coastal waters. *Coast. Eng.* 58, 92–1012.